ARTICLES

Time-resolved experiments on light diffusion in anisotropic random media

Diederik S. Wiersma,* Alessandro Muzzi, Marcello Colocci, and Roberto Righini
European Laboratory for Non-Linear Spectroscopy and Instituto Nazionale per la Fisica della Materia, Largo Enrico Fermi 2 (Arcetri), 50125 Florence, Italy
(Received 25 May 2000)

Multiple light scattering in isotropic and anisotropic media is studied experimentally with an optical gating technique, as commonly used in fluorescence spectroscopy. The experimental setup permits an accurate analysis of the propagation of a short light pulse through disordered or partially ordered media. The diffusion constant of some isotropic systems is reported, and the anisotropy in the diffusion constant for light diffusion through liquid crystals is observed. For the time-resolved data, good agreement with diffusion theory is found in all cases, including the liquid crystal in the nematic phase.

PACS number(s): 61.30.Gd, 42.25.Bs, 42.70.Df, 78.30.Ly

I. INTRODUCTION

The propagation of electromagnetic waves in complex dielectric structures is full of surprises. Of interest are periodically ordered mesoscopic systems like photonic crystals on one side, and disordered materials like powders or suspensions of microspheres on the other. Ordered mesoscopic dielectric systems, with a lattice constant comparable to the wavelength, behave like a crystal for light waves. At high enough refractive index contrast, a photonic band gap is expected to occur [1,2]. For lower dimensional systems, a photonic band gap for both microwaves and near infrared light has been observed experimentally [3], and for true three-dimensional (3D) systems inverse-opal structures of high refractive index material like TiO_2 look very promising in the optical regime [4]. The high refractive index contrast needed to obtain a full photonic bandgap in 3D can be obtained with inverse-opal structures of silicon [5]. The realization of photonic band gap materials is interesting for applications in optical devices like optical switches and complex waveguides [2].

Light waves in disordered materials, on the other hand, are randomly scattered and undergo a diffusive type of transport. What makes disordered systems interesting is that interference effects can survive random multiple scattering. Examples of such interference effects are coherent backscattering or weak localization [6] and short and long range intensity correlations [7]. Light propagation in disordered systems shows many similarities with the propagation of electrons in (semi)conductors, and various phenomena that are common for electron transport have now also been found to exist for light waves [8]. Important examples are the photonic Hall effect [9], optical magnetoresistance [10], Anderson localization [11], and universal conductance fluctuations [12]. Important applications of multiple light scattering include medical imaging [13] and diffusing wave spectroscopy [14].

Liquid crystals in the nematic phase are opaque and therefore also give rise to multiple light scattering. This allows coherent backscattering to be observed from large nematic systems [15]. The partial ordering of the nematic phase leads to an anisotopic scattering function, which makes nematic liquid crystals fundamentally different from common random media. This anistropy in the scattering cross section leads, for large enough samples, to an anisotropic diffusion process, and monodomain nematics are therefore ideal systems for studying anisotropic multiple light scattering. Anisotropic light diffusion has recently been observed in elegant cw experiments by Kao *et al.* [16], and later in time-resolved experiments [17], both on large monodomain nematics. A wide scale of inspiring theoretical work is available on light propagation in opaque liquid crystals [18].

II. LIGHT SCATTERING IN NEMATICS

A. Single scattering

The nematic phase of a liquid crystal is characterized by a (global) alignment of the molecules in a certain direction, called the nematic director **n**, and an otherwise translational disorder. Under normal circumstances, a large liquid crystal sample that is brought into the temperature range corresponding to the nematic phase (e.g., 297–308 K for the liquid crystal *p*-penthyl-*p'*-cyanobiphenyl or 5CB) will form a polydomain nematic phase. With the help of an external magnetic or electric field, it is possible to achieve large monodomain nematics, in which the molecules are aligned in the same direction over the whole sample volume. The remaining local fluctuations of the nematic director cause the nematic phase to be relatively strongly scattering. The correlation length of the director fluctuations depends on the external field and in the case of a magnetic field of strength H is given by $\xi = \sqrt{K_1/\Delta\chi H^2}$, where K_1 is the Frank elastic constant for splay deformations and $\Delta\chi$ is the anisotropy in the diamagnetic susceptibility [19]. The physical interpreta-

*Email address: wiersma@lens.unifi.it

tion of ξ is that any perturbation somewhere inside the sample will cause a distortion of the nematic director over a range ξ. For zero magnetic field, the correlation length ξ, also called the magnetic coherence length, diverges. Due to the partial order of the nematic phase, the scattering cross section σ for a light wave incident on or propagating in the liquid crystal will depend on the incoming and outgoing polarization and propagation directions relative to the direction of the nematic director. The single scattering differential cross section for a small volume V of liquid crystal is given by [19,20]

$$\sigma_{\mathrm{sc}} = Vs\left(\frac{\Delta\epsilon k^2}{4\pi}\right)^2 \sum_{\alpha=1,2} \frac{k_b T (i_\alpha f_z + i_z f_\alpha)^2}{K_\alpha q_\perp^2 + K_3 q_\parallel^2 + K_1 \xi^{-2}}. \qquad (1)$$

Here $\mathbf{q}=\mathbf{k_f}-\mathbf{k_i}$ is the scattering wave vector with $\mathbf{k_i}$ the initial and $\mathbf{k_f}$ the final wave vector of the scattered light wave, K_1, K_2, and K_3 are the Frank elastic constants for splay, twist, and bend deformations respectively, $\mathbf{i}$ and $\mathbf{f}$ are unit vectors representing the initial and final polarization directions, V is the scattering volume, k_b is the Boltzman constant, and T is the temperature. The vector $\mathbf{n}_0$ is the average value of the nematic director and is chosen in the $\hat{\mathbf{z}}$ direction. The directions $\alpha=1,2$ refer to the unit vectors $\mathbf{e}_1$, $\mathbf{e}_2$ of the director fluctuations eigenmodes: $\mathbf{e}_1$ and $\mathbf{e}_2$ are in the x-y plane with $\mathbf{e}_2$ normal to $\mathbf{q}$ and $\mathbf{e}_1$ normal to $\mathbf{e}_2$. The projections $q_\perp$ and $q_\parallel$ are the components of $\mathbf{q}$ respectively perpendicular and parallel to $\mathbf{n}_0$. A light wave with polarization perpendicular to both $\mathbf{k}$ and $\mathbf{n}_0$ is called an ordinary wave (o), while the case where the polarization lies in the plane defined by $\mathbf{k}$ and $\mathbf{n}_0$ is referred to as extraordinary (e). The system will be birefringent with a refractive index $m_o=\sqrt{\epsilon_o}=\sqrt{\epsilon_\perp}$ for a light wave with polarization perpendicular to $\mathbf{n}_0$ and refractive index $m_e=\sqrt{\epsilon_e}=\sqrt{\epsilon_\parallel}$ for the limiting extraordinary case of a wave with polarization parallel to $\mathbf{n}_0$. For 5CB at a wavelength of 405 nm we have $m_o=1.571$ and $m_e=1.811$ [21].

From Eq. (1), we see that the scattered intensity is zero for conserving polarization channels with respect to the direction of the nematic director: if the incoming polarization is in the x-y plane, the outgoing polarization has to have a nonzero component in $\hat{\mathbf{z}}$ and vice versa. Furthermore we see from Eq. (1) that the cross section diverges for $\mathbf{q}=\mathbf{0}$ at zero magnetic field. To illustrate its complicated and rich structure, we have plotted σ_{sc} in Fig. 1 for various incoming wave vectors and polarizations. The nematic director is in all cases along $\hat{\mathbf{z}}$. In the upper two cases $\mathbf{k_i}=k\,\hat{\mathbf{z}}$, the incoming polarization is ordinary, and the outgoing polarization is extraordinary. In Fig. 1(a) the incident polarization is along $\hat{\mathbf{y}}$, whereas in Fig. 1(b) it is along $\hat{\mathbf{x}}$. The intensity in the exact forward scattering direction is zero due to the above polarization rules. The ellipsoidal shape is a consequence of K_1 and K_2 having different values, which is also the reason for Fig. 1(a) and 1(b) being distinct. With $\mathbf{k_i}=k\,\hat{\mathbf{z}}$ and ordinary incoming and outgoing polarization, the cross section is always zero. In Figs. 1(c) and 1(d), the incident wave vector is along $\mathbf{x}$. For Fig. 1(c), the incident polarization is ordinary (along $\mathbf{y}$), while the outgoing polarization is extraordinary

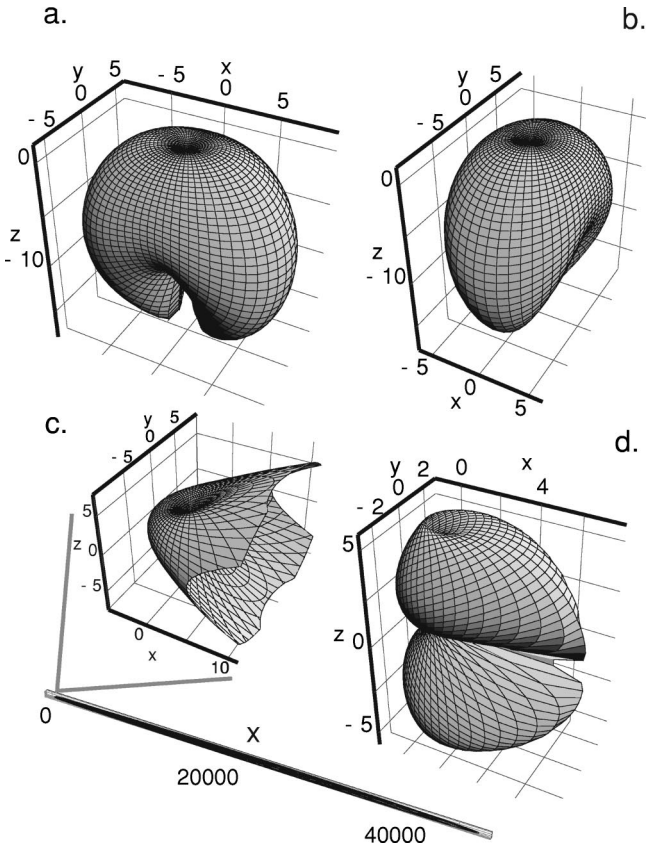

FIG. 1. Spherical plot of the single scattering cross section σ_{sc} of the liquid crystal 5CB in the nematic phase, as given by Eq. (1). ($K_1=0.79K_3$, $K_2=0.43K_3$, $K_3=5.3\times10^{-7}$ dyne, $\Delta\epsilon=\epsilon_\parallel-\epsilon_\perp=0.811\,68$, $\Delta\chi=0.95\times10^{-7}$, $H=0.5$ T, which yields $\xi=4.2$ μm.) The nematic director is along $\hat{\mathbf{z}}$. In the upper two plots the incoming beam is incident along $\hat{\mathbf{z}}$, in the lower plots along $\hat{\mathbf{x}}$. In the upper plots the outgoing polarization is extraordinary. Upper left (a), incident polarization in $\hat{\mathbf{y}}$, upper right (b) incident polarization in $\hat{\mathbf{x}}$. Lower left (c), incident polarization ordinary, final polarization extraordinary or vice versa (identical). Note the strongly forward peaked scattering in this case, characteristic of the nematic phase. The enlargement shows the region around the origin. Lower right (d), both incident and final polarization extraordinary.

(along $\mathbf{z}$ for exact forward scattering). The case with incident polarization extraordinary and outgoing ordinary is identical. We can see that the scattering is extremely pointed in the forward direction for this case. This leads to the large difference between the transport mean free path and the scattering mean free path for nematics [18]. The inset in Fig. 1(c) shows an enlargement of the region around the origin, from which we can see that only the cross section for $\mathbf{k_f}=k\,\hat{\mathbf{z}}$ is really zero. In Fig. 1(d), we have plotted the peculiar case of extraordinary incoming and outgoing polarizations, which leads to a nonzero cross section only for scattering out of the x-y plane. With ordinary incoming and outgoing polarizations, the cross section is always zero.

For isotropic systems, the scattering mean free path is usually defined as the average distance between two scattering events and is inversely proportional to the scattering differential cross section. In a nematic, the scattering cross section depends on both incoming wave vector and polarization. For ordinary (o) [extraordinary (e)] incoming polarization,

the scattering mean free path is

$$\ell_{i=o,e}^{-1}=\sum_{f=o,e}\int d\Omega\, V^{-1}\sigma_{\mathrm{sc}}(i=o,e), \tag{2}$$

where the sum is over both output polarization channels. Without absorption, the incoming coherent beam will be attenuated in the usual way via $I_{o,e}(z)=I_0\exp(-z/\ell_{i=o,e})$. Due to the divergence of the cross section, the scattering mean free path loses its meaning at zero magnetic field.

B. Multiple scattering

If the dimensions of the system greatly exceed the scattering mean free path, it will become opaque and multiple scattering will dominate. In an isotropic system, the light waves will then perform a random walk with an average step length and velocity. The average step length is given by the transport mean free path ℓ^* and the velocity by the transport velocity v_e [22]. The transport mean free path is defined as the average distance over which a light wave completely loses memory of its original propagation direction. For isotropic point scatterers ℓ^* is equal to ℓ. If the single scattering function is, for instance, pointed in the forward direction, ℓ^* can be much bigger than ℓ and is given by $\ell^*=\ell/(1-\langle\cos\theta\rangle)$, with $\langle\cos\theta\rangle$ the average scattering angle.

In a thick monodomain nematic, a propagating light wave will perform an isotropic random walk with anisotropic step length and velocity. One can distinguish between $\ell_\perp^*$ and $\ell_\parallel^*$, the transport mean free paths for propagation directions perpendicular and parallel to **n**, and $v_\perp$ and $v_\parallel$ the velocities in the corresponding propagation directions.

Often the random walk picture can be simplified into a diffusion process with diffusion constant D. In the (3D) isotropic case the diffusion constant simply relates to ℓ^* and v_e as

$$D=1/3v_e\ell^*. \tag{3}$$

In practice, the diffusion approximation turns out to work surprisingly well for most isotropic disordered media. It is important to note that in a time-resolved experiment one can measure the diffusion constant D, whereas in a static experiment one can obtain to the transport mean free path ℓ^*.

If we wish to use the diffusion approximation to describe light propagation in nematic liquid crystals, we have to use an anisotropy diffusion equation. Note, however, that by assuming a diffusion process, we assume that all microscopic details of the multiple scattering process can be incorporated in a single parameter **D**, which in the complicated case of nematic liquid crystals is not obvious. For an anisotropic medium the diffusion equation is

$$\frac{\partial W(\mathbf{r},t)}{\partial t}=\boldsymbol{\nabla}\cdot\mathbf{D}\boldsymbol{\nabla}W(\mathbf{r},t)-\tau_{\mathrm{i}}^{-1}W(\mathbf{r},t)+S(\mathbf{r},t), \tag{4}$$

with $W(\mathbf{r},t)$ the energy density, $S(\mathbf{r},t)$ a source function, and τ_{i} the inelastic or absorption time, which is the characteristic time over which light is absorbed inside the sample. For simplicity we assume the absorption time to be isotropic. However, in the case where the absorption is direction dependent, τ_{i} can be read as an appropriate weighted average over all directions. Choosing the nematic director along one of the coordinate axis, the distinct elements of the diffusion tensor will be $D_\perp$ and $D_\parallel$. It is not intuitively clear what is now the relation between the anisotropic random walk parameters and D. We conjecture that we can write

$$D_\parallel=\frac{1}{3}v_\parallel\ell_\parallel,\quad D_\perp=\frac{1}{3}v_\perp\ell_\perp, \tag{5}$$

which can be read as a definition of $v_\perp$ and $v_\parallel$.

The diffusion equation (4) can be easily solved for given boundary conditions. In the case of a slab geometry we have $W(\mathbf{r},t)=0$ at $z=-z_0$ and $z=L+z_0$, with L the physical thickness of the slab. The distance z_0 is called the extrapolation length and depends on the refractive index mismatch between sample and surrounding medium [23]:

$$z_0=2/3\ell_z(1+R)/(1-R), \tag{6}$$

with R the average reflectivity at the sample interface and ℓ_z the transport mean free path in the z direction. We assume that the incident pulse is fully scattered at a depth ℓ_z and, for symmetry, that the last scattering event takes place at $z=L-\ell_z$. The time evolution of the transmitted intensity is given by Fick's law [24] $[I_{\mathrm{tr}}=-D_{zz}\boldsymbol{\nabla}W(\mathbf{r},t)|_{z=L-\ell_z}]$ and reads after solving Eq. (4) with the source function $S(\mathbf{r},t)=\delta(x)\,\delta(y)\,\delta(z-\ell_z)\,\delta(t)$ [25]

$$I_{\mathrm{tr}}=\frac{I_0\exp(-t/\tau_i)\exp(-\Delta x^2/4D_{xx}t)\exp(-\Delta y^2/4D_{yy}t)}{\pi^{3/2}(4t)^{5/2}\sqrt{D_{xx}D_{yy}D_{zz}}}\times\sum_{n=-\infty}^{+\infty}A\exp(-A^2/4D_{zz}t)-B\exp(-B^2/4D_{zz}t), \tag{7}$$

with $A=(1-2n)(L+2z_0)-2(z_0+\ell_z)$ and $B=(2n+1)(L+2z_0)$, and where Δx and Δy denote the shift of the incoming beam in x and y, respectively. Note that in the limit of long t and in the absence of absorption, the transmitted intensity falls off as an exponential with time constant $\tau=(L+2z_0)^2/D_{zz}\pi^2$.

If Δx and Δy are chosen zero, the transmission will depend only on D_{zz}. This means that $D_\perp$ and $D_\parallel$ can be measured by orienting the nematic director either perpendicular (homeotropic alignment) or parallel (planar alignment) to the plane of the slab ($D_{zz}=D_\perp$ or $D_{zz}=D_\parallel$ respectively). If, on the other hand, the incident beam is translated over Δx or Δy, the transmitted intensity will also depend (weakly) on the xx or yy components of **D**, which allows one to measure $D_\perp$ and $D_\parallel$ in principle in one measurement, using a planar aligned sample.

III. EXPERIMENTAL CONFIGURATION

We have performed time-resolved measurements on the diffuse transmission through various samples, using an optical gating technique as often applied in time-resolved fluorescence spectroscopy [26]. This method is based on sum-

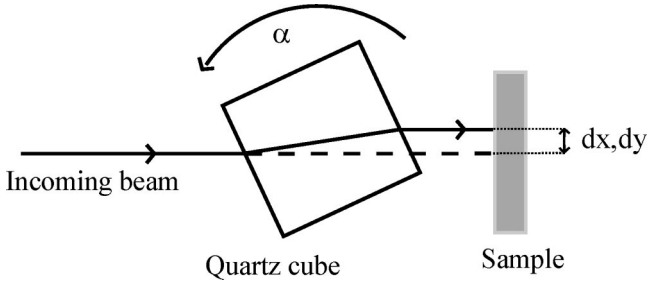

FIG. 2. Detail of the experimental setup for recording the time-resolved diffuse transmission through opaque media. The incident probe beam can be translated by rotating a quartz cube. Rotation is possible both in the plane of the drawing and perpendicular to it, which allows for varying both Δx and Δy.

frequency generation in a nonlinear crystal where the signal light (fluorescence or diffuse scattering) is mixed with a high intensity gate pulse. This method has the advantage that the time resolution, in principle, is limited only by the pulse width of the probe and gate pulses. In our case the limiting factor on the time resolution (2.4 ps) was the thickness of the nonlinear crystal that was used to generate the sum-frequency signal.

The samples had a slab geometry, with the slab oriented in the x-y plane and the laser incident along $\hat{\mathbf{z}}$. The laser beam was narrow (1 mm) and the transmitted light through the slab was recorded around $x=y=0$ through a diaphfragm of 1 mm diameter. The incident laser could be translated in x and y by rotating a block of quartz. (See Fig. 2.) We followed two strategies to observe the anisotropy in the diffusion constant. In the first case we kept the incident beam fixed at $x=y=0$ and varied the orientation of the liquid crystal inside the sample cell. This was done by applying the magnetic field either in the $\hat{\mathbf{x}}$ or $\hat{\mathbf{z}}$ direction, which yields a planar, respectively, homeotropic alignment of the nematic director. In a second set of measurements we kept a fixed planar alignment and translated the incoming beam either in x or in y.

The details of the experimental setup are shown in Fig. 3. Our laser source is an amplified Ti:sapphire laser operating at 1 kHz, wavelength 810 nm, and pulse duration 50 fs. A low intensity (0.1 mW) probe beam at 405 nm is generated by frequency doubling in a Beta-Barium Borate (BBO) crystal.[1] The remaining power (400 mW) of the 810 nm light is used as gate beam. The probe beam has a diameter of 1 mm and is incident on the sample via a rotatable quartz cube. The scattered light transmitted by the sample is largely blocked by a 1 mm diaphragm, centered behind the sample. The transmitted light that passes the diaphragm is mixed with the gate beam in a BBO crystal to generate a sum-frequency signal at a wavelength of 270 nm. A double bandpass filter (peaked at 270 nm) is placed in front of the photomultiplier tube (PMT). The three wavelengths that exit the BBO crystal are separated by a prism in order to avoid problems from the high intensity gate beam in the bandpass filters. The gate pulse is delayed via an electronically controlled delay line. The probe beam is chopped by a mechanical chopper at 500 Hz (synchronized with the laser), and a lock-in amplifier is used to detect the PMT signal. The sample cell is placed between the (10 cm diameter) pole shoes of an electromagnet. In the case of a homeotropic alignment four small extra mirrors (not shown) are used to allow the sample to be perpendicular to the field.

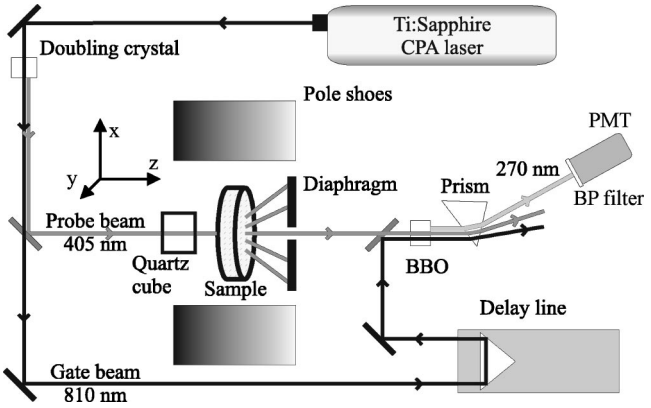

FIG. 3. Experimental setup to record the time evolution of the transmission of a short probe pulse through a diffusely scattering medium. The probe pulse is generated by frequency doubling the output of a CPA Ti:sapphire laser (wavelength 810 nm, pulse duration 50 fs, repetition rate 1 kHz), and is incident on the sample via a quartz cube to allow lateral translation of the probe beam. The average power of the probe is 0.1 mW. The 1 mm diameter diaphragm is placed directly after the sample cell. The diffuse transmission that passes the diaphragm is mixed in a nonlinear crystal (BBO) with a high intensity (400 mW) gate beam, to generate a sum-frequency signal at 270 nm wavelength. A prism is used to separate the signal light from both gate and probe beams, and additional bandpass (BP) filters are used in front of the photomultiplier tube (PMT) to select a narrow wavelength band around 270 nm. The sample is placed between the (10 cm diameter) poles of an electromagnet. All mounts are of plastic or aluminum, to avoid distortion of the magnetic field. By varying the delay of the gate beam, the time evolution of the transmitted signal can be recorded. A chopper is placed in the probe beam (not shown) and a lock-in amplifier is used to record the PMT signal.

IV. EXPERIMENTAL RESULTS

With the above setup we have performed time-resolved transmission measurements on various opaque systems, both isotropic and anisotropic. Two examples of measurements on isotropic random media are shown in Fig. 4. In the top graph, the results are shown for the transmission through a solid opaque sample of Teflon; in the bottom graph for the transmission through a suspension of polyester microspheres in water. The solid curve is obtained from diffusion theory using Eq. (7), taking into account internal reflection at the front and rear sample interfaces. By fitting the complete theoretical curve to the data one can obtain both the diffusion constant D and the absorption time τ_i. In the absence of absorption, τ_i goes to infinity and Eq. (7) becomes independent of τ_i. In practice, Eq. (7) becomes insensitive to τ_i if τ_i is much larger than $\tau=(L+2z_0)^2/D_{zz}\pi^2$.

We can see that, for both the solid sample and the micro-

[1]The probe pulse is stretched to 1 ps, to avoid high peak intensities that could give rise to two photon absorption in the liquid crystal samples.

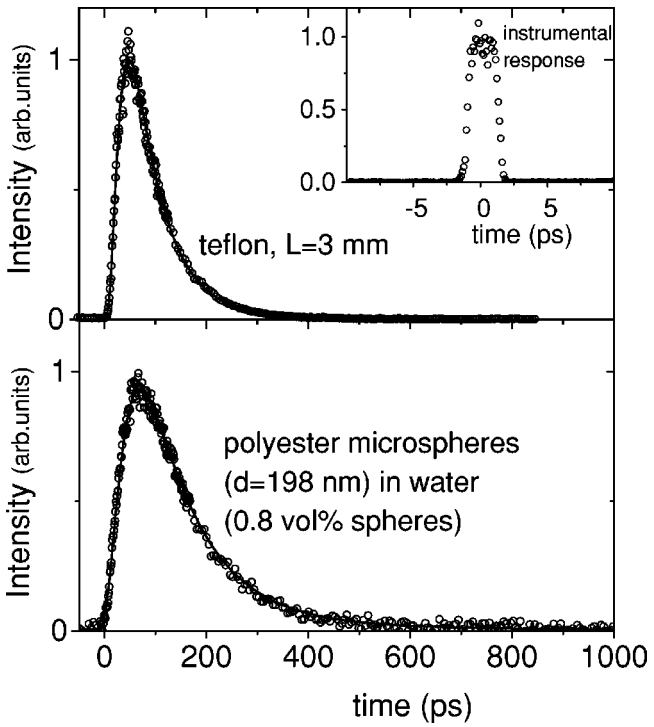

FIG. 4. Diffuse transmitted intensity versus time. Upper graph: Teflon, sample thickness 3 mm; lower graph: 0.8 vol % suspension of polyester microspheres (diameter = 198 nm, 1.8% cv) in water, sample thickness 5.2 mm. The solid line is a fit from diffusion theory [Eq. (7)], taking into account internal reflection via Eq. (6). The xx, yy, and zz components of the diffusion constant are assumed to be equal in the case of Teflon and polyester microspheres. Upper graph: $D=1.22\times10^4$ m^2/s. (Average refractive index $m=1.4$, $R=0.48$ [23].) The absorption time for Teflon is $\tau_i=0.7$ ns. Lower graph: $D=1.95\times10^4$ m^2/s, using an average refractive index contrast between sample windows (quartz) and water of $m=1.095$, which gives $R=0.135$. Inset: time response obtained by substituting the sample with an ultrathin lens-cleaning paper. Time resolution 2.4 ps.

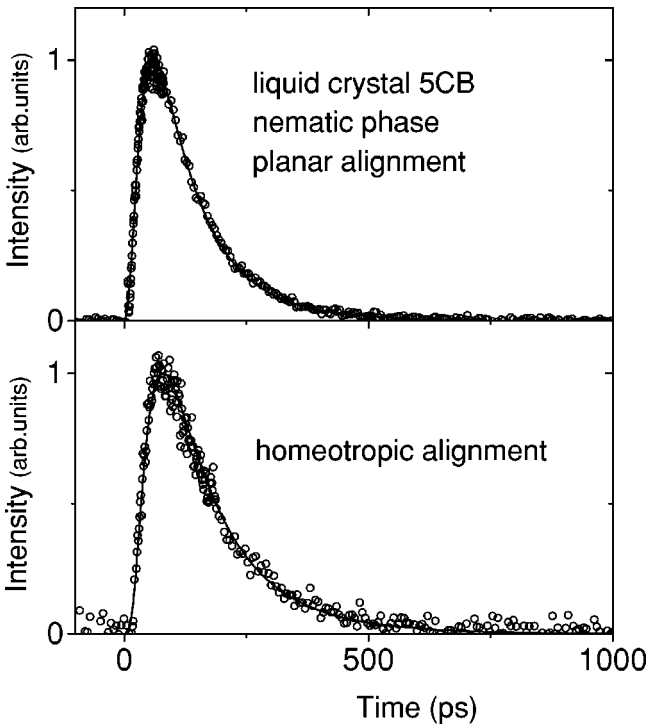

FIG. 5. Comparison of the transmitted intensity versus time between a planar (upper) and homeotropic (lower) alignment of the liquid crystal 5CB in the nematic phase. (Incident polarization in $\hat{\mathbf{y}}$, observed polarization in $\hat{\mathbf{x}}$, $T=300$ K, $B=0.5$ T.) The solid line is obtained from Eq. (7), taking into account internal reflection. (Refractive index contrast at the sample window $m=1.691/1.47=1.15$, which gives $R=0.21$.) From the planar alignment we find $D_{zz}=D_\perp=(3.62\pm0.15)\times10^4$ m^2/s, and from the homeotropic alignment $D_{zz}=D_\parallel=(4.56\pm0.18)\times10^4$ m^2/s. The anisotropy in the diffusion constant is therefore $D_\parallel/D_\perp=1.26\pm0.07$.

sphere suspension, the data correspond well with diffusion theory. The diffusion constant as obtained from these measurements for Teflon and the polyester microsphere suspension (0.8 vol % spheres, diameter 198 nm in water), is, respectively, $D=1.22\times10^4$ m^2/s and $D=1.95\times10^4$ m^2/s. One can assume that the transport velocity for the low concentration of microspheres in water is very close to the phase velocity of light in water at that wavelength ($v=c_0/1.343=2.234\times10^8$ m/s), which gives, via Eq. (3), a transport mean free path of 0.26 mm. This value is of the same order as the expected transport mean free path of the nematic phase of the liquid crystal 5CB. The absorption time obtained for teflon is $\tau_i=0.7$ ns. For the polyester microspheres the absorption time was too long to be determined within our noise level (i.e., negligible absorption on the time scale of the measurement).

The inset of Fig. 4 shows the time resolution of the setup as obtained by substituting the sample with an ultrathin lens-cleaning paper. The (strong) coherent beam that exits the sample in this case (under a slight angle) was thoroughly blocked. The resolution is about 2.4 ps. Note that the flattened top of the resolution curve is not due to saturation, but is probably caused by the large thickness (6 mm) of the sum-frequency crystal. The typical decay times (100 ps or more) for our samples of interest are much larger than the resolution.

In order to study the anisotropy in the diffusion constant, we have performed transmission measurements on the liquid crystal *p*-penthyl-*p′*-cyanobiphenyl , which is nematic at room temperature and has its nematic-isotropic phase transition at 308 K. For every experiment, the sample was heated to 318 K and let cool down to 300 K overnight in a magnetic field of 0.5 T to obtain monodomain samples. The magnetic field was generated by an electromagnet with large 10 cm diameter pole shoes, in order to assure homogeneity of the field. We found that for achieving a homogeneous homeotropic alignment cooling slowly was important, while the monodomain planar aligment could also be achieved within tens of minutes. In addition it was observed repeatedly that a planar aligned sample stayed visually the same after switching off the magnetic field, suggesting that it stays for an appreciable time in a monodomain nematic phase even without external field. Only by removing the sample from the setup and agitating it strongly can one observe that the sample ''breaks up'' into several zones of millimeter size. This latter behavior was observed for a homeotropic alignment immediately after switching off the external field, already with modest physical disturbance of the sample. The

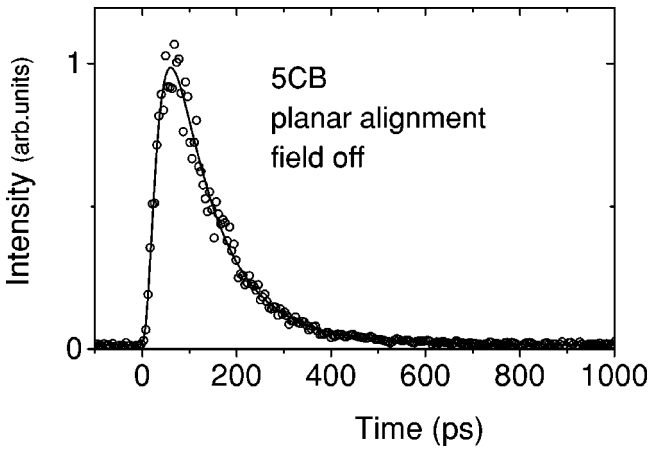

FIG. 6. Transmitted intensity of a planar aligned sample, immediately after switching off the magnetic field. At zero field, the magnetic coherence length diverges. Nevertheless, the correspondence between data and diffusion theory (solid line) is very good. We find for the perpendicular component of the diffusion constant $D_{zz}=D_{\perp}=3.54\times10^{4}$ m^2/s, which equals, within the experimental error, $D_{\perp}$ as measured before.

sample was contained in a (quartz) glass cell (with Teflon side wall) of 25 mm diameter. The sample cell was temperature controlled with an accuracy better than 1 K.

The results of the time-resolved measurements for planar and homeotropic alignment of the director are shown in Fig. 5. The incoming beam was kept fixed at $x=y=0$. The scattering is stronger for the planar alignment (upper data set) than for the homeotropic alignment (lower data set). Therefore, in order to have about the same optical thickness in both cases, we chose the physical thickness of the planar aligned sample as $L=6.3$ mm and of the homeotropic aligned sample as $L=7.9$ mm. We have performed all experiments with both vertical and horizontal incoming polarization and found no polarization dependence in the diffuse transmission.

The solid line is obtained from diffusion theory, using Eq. (7), taking into account internal reflection. We see that the correspondence between data and theoretical curves is again very good. From a fit of Eq. (7) to the data we find for the planar alignment $D_{zz}=D_{\perp}=(3.62\pm0.15)\times10^{4}$ m^2/s, and for the homeotropic alignment $D_{zz}=D_{\parallel}=(4.56\pm0.18)\times10^{4}$ m^2/s. The anisotropy in the diffusion constant is therefore $D_{\parallel}/D_{\perp}=1.26\pm0.07$. These results are in agreement with the theoretical predictions in Ref. [18].

In the magnetic field that we use to keep our sample in a monodomain nematic phase, the magnetic coherence length ξ is of the order of several micrometers. (At 0.5 T field strength, $\xi=4.2$ μm.) As long as ξ is much smaller than the scattering mean free path, one can picture the random walk as a series of independent single scattering events. The magnetic coherence length diverges, however, at zero field so that at low fields ξ can become of the order of millimeters. In addition, the scattering mean free path as defined by Eq. (2) goes to zero. In this regime the simple picture of a random walk as a sequence of individual single scattering events apparently breaks down.

The ease with which the planar phase is formed and apparently maintained after switching off the magnetic field

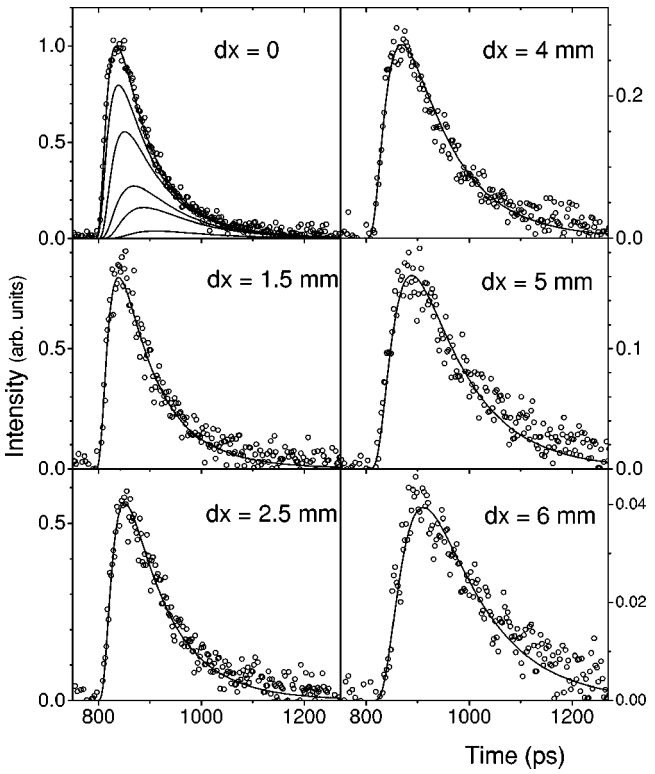

FIG. 7. Comparison of the time-resolved transmission at various lateral displacements of the incoming beam. Sample: 0.2 wt % of $BaSO_4$ powder in water. From the $\Delta x=0$ measurement we find $D=4.73\times10^{4}$ m^2/s which gives, using $v=c_0/1.343=2.234\times10^{8}$ m/s, a transport mean free path of $\ell^*=0.635$ mm. (Refractive index contrast at sample interface $m=1.343/1.470=1.0943$, $R=0.135$.) The same value of $D=4.73\times10^{4}$ m^2/s is used for all theoretical curves. In the upper left plot all theoretical curves are plotted together, to illustrate the evolution of the transmission upon increasing Δx.

allowed us to test the effect of increasing magnetic coherence length. In Fig. 6, we show the results of the time-resolved transmission (incoming beam fixed at $x=y=0$) on a planar sample, just after (slowly) switching off the external field. With a Hall probe it was checked that no residual field due to magnetization of nearby metal objects was present. Surprisingly enough, we observe in Fig. 6 that the time-resolved transmission does not change appreciably at zero field. The solid line is obtained from Eq. (7) and corresponds to $D_{zz}=3.54\cdot10^{4}$ m^2/s which is, within the experimental error, equal to $D_{\perp}$ as found above. The correspondence between data and theoretical curve is again very good. The diffusion approximation apparently is adequate to describe the diffuse transmission through large nematics, even at zero field, despite the divergence of ξ.

To check the consistency of our results, we have performed time-resolved transmission measurements with a translated input beam $(x,y\neq0)$, in which case the transmitted intensity depends on both D_{zz} and either D_{xx} or D_{yy}. In Fig. 7, we show the time-resolved transmission through a suspension of $BaSO_4$ powder in water, at various lateral translations Δx of the incoming beam. By comparing the data at $\Delta x=0$ with Eq. (7), we find $D_{zz}=D=4.73\times10^{4}$ m^2/s. Using the same value for D_{xx} and D_{zz} we find excellent correspondence between data and theoretical

curves for all Δx, without free fitting parameters. In the upper left graph, we have plotted all theoretical curves together on the same scale, which illustrates how the intensity profile changes upon increasing Δx.

By choosing a suitable orientation of the nematic director with respect to the translation direction, one can measure in this way both $D_\perp$ and $D_\parallel$ at the same time. The dependence on D_{xx} and D_{yy} is weak, however, which does not allow for an accurate determination of $D_\parallel$. The reason for this is that the decay of the time-resolved transmission is mainly determined by D_{zz}, even for large values of Δx. In Ref. [17], we gave the results for 5CB in the nematic phase oriented along $\hat{\mathbf{x}}$ (planar alignment) and the input beam translated to $x = 6$ mm. To check the consistency of our data we used the previously determined value of $D_\perp = 3.62 \times 10^4$ m^2/s. In that case we find for the parallel component $D_\parallel = (4.40 \pm 0.50) \times 10^4$ m^2/s, which is consistent with the data measured in the homeotropic geometry.

ACKNOWLEDGMENTS

We thank Bart van Tiggelen, Holger Stark, Tom Lubensky, Cecil Chung, and Arjun Jodh for stimulating discussions, and Cecilia Gambi and Donatella Senatra for the use of the electromagnet. This work was supported by the EC under Contract No. HPRI-CT1999-00111 and DSW with the Marie Curie Grant No. ERBFMBICT972107.

[1] E. Yablonovitch, Phys. Rev. Lett. **58**, 2059 (1987); S. John, *ibid.* **58**, 2486 (1987).

[2] *Photonic Bandgap Materials*, edited by C.M. Soukoulis (Kluwer, Dordrecht, 1996); J.D. Joannopoulos, R.D. Meade, and J.N. Winn, *Photonic Crystals* (Princeton University Press, Princeton, NJ, 1995).

[3] S.L. McCall, P.M. Platzman, R. Dalichaouch, D. Smith, and S. Schultz, Phys. Rev. Lett. **67**, 2017 (1991); R.D. Meade, K.D. Brommer, A.M. Rappe, and J.D. Joannopoulos, Appl. Phys. Lett. **61**, 495 (1992); U. Grüning, V. Lehmann, S. Ottow, and K. Busch, *ibid.* **68**, 747 (1996).

[4] A. Imhof and D.J. Pine, Nature (London) **389**, 948 (1997); B.T. Holland, C.F. Blanford, and A. Stein, Science **281**, 538 (1998); J.E.G.J. Wijnhoven and W.L. Vos, *ibid.* **281**, 802 (1998); A.A. Zakhidov, R.H. Baughman, Z. Iqbal, Ch. Cui, I. Khayrullin, S.O. Dantas, J. Marti, and V.G. Ralchenko, *ibid.* **282**, 897 (1998); M.S.T. Thijssen, R. Sprik, J.E.G.J. Wijnhoven, M. Megens, T. Narayanan, A. Lagendijk, and W.L. Vos, Phys. Rev. Lett. **83**, 2730 (1999).

[5] A. Blanco, E. Chomski, S. Grabtchak, M. Ibisate, S. John, S.W. Leonard, C. Lopez, F. Meseguer, H. Miguez, J.P. Mondia, G.A. Ozin, O. Toader, and H.M. van Driel, Nature (London) **405**, 437 (2000).

[6] Y. Kuga and A. Ishimaru, J. Opt. Soc. Am. A **8**, 831 (1984); M.P. van Albada and A. Lagendijk, Phys. Rev. Lett. **55**, 2692 (1985); P.E. Wolf and G. Maret, *ibid.* **55**, 2696 (1985).

[7] N. Garcia and A.Z. Genack, Phys. Rev. Lett. **63**, 1678 (1989); M.P. van Albada, J.F. de Boer, and A. Lagendijk, *ibid.* **64**, 2787 (1990).

[8] See, for instance, P. Sheng, *Introduction to Wave Scattering, Localization, and Mesoscopic Phenomena* (Academic Press, San Diego, 1995).

[9] B.A. van Tiggelen, Phys. Rev. Lett. **75**, 422 (1995); G.L.J.A. Rikken and B.A. van Tiggelen, Nature (London) **381**, 54 (1996).

[10] A. Sparenberg, G.L.J.A. Rikken, and B.A. van Tiggelen, Phys. Rev. Lett. **79**, 757 (1997).

[11] R. Dalichaouch, J.P. Armstrong, S. Schultz, P.M. Platzman, and S.L. McCall, Nature (London) **354**, 53 (1991); A.Z. Genack and N. Garcia, Phys. Rev. Lett. **66**, 2064 (1991); D.S. Wiersma, P. Bartolini, A. Lagendijk, and R. Righini, Nature (London) **390**, 671 (1997).

[12] F. Scheffold and G. Maret, Phys. Rev. Lett. **81**, 5800 (1998).

[13] A. Yodh and B. Chance, Phys. Today **48**(3), 34 (1995).

[14] G. Maret and P.E. Wolf, Z. Phys. B **65**, 409 (1987); D.J. Pine, D.A. Weitz, P.M. Chaikin, and E. Herbolzheimer, Phys. Rev. Lett. **60**, 1134 (1988).

[15] D.V. Vlasov, L.A. Zubkov, N.V. Orekhova, and V.P. Romanov, Pis'ma Zh. Éksp. Teor. Fiz. **48**, 86 (1988) [JETP Lett. **48**, 91 (1988)]; H.K.M. Vithana, L. Asfaw, and D.L. Johnson, Phys. Rev. Lett. **70**, 3561 (1993).

[16] M.H. Kao, K.A. Jester, A. Yodh, and P.J. Collins, Phys. Rev. Lett. **77**, 2233 (1996).

[17] D.S. Wiersma, A. Muzzi, M. Colocci, and R. Righini, Phys. Rev. Lett. **83**, 4321 (1999).

[18] V.P. Romanov and A.N. Shalaginov, Opt. Spektrosk. **64**, 1299 (1988) [Opt. Spectrosc. **64**, 774 (1988)]; B.A. van Tiggelen, R. Maynard, and A. Heiderich, Phys. Rev. Lett. **77**, 639 (1996); H. Stark and T.C. Lubensky, *ibid.* **77**, 2229 (1996); Phys. Rev. E **55**, 514 (1997); B.A. van Tiggelen, A. Heiderich, and R. Maynard, Mol. Cryst. Liq. Cryst. Sci. Technol., Sect. A **293**, 205 (1997); B.A. van Tiggelen, *ibid.* **321**, 197 (1998); H. Stark, *ibid.* **321**, 403 (1998); B.A. van Tiggelen and H. Stark, Rev. Mod. Phys. (to be published).

[19] P.G. de Gennes and J. Prost, *The Physics of Liquid Crystals*, 2nd ed. (Oxford, New York, 1993).

[20] D. Langevin, Solid State Commun. **14**, 435 (1974); D. Langevin and M.-A. Bouchiat, J. Phys. (Paris), Colloq. **C1**, 197 (1975). S. Chandrasekhar, *Liquid Crystals* (Cambridge Univ. Press, Cambridge, 1977); A.Y. Val'kov and V.P. Romanov, Zh. Éksp. Teor. Viz. **82**, 1777 (1982) [Sov. Phys. JETP **56**, 1028 (1983)].

[21] Shin Tson Wu, Chiung Sheng Wu, M. Warenghem, and M. Ismaili, Opt. Eng. **32**, 1775 (1993).

[22] M.P. van Albada, B.A. van Tiggelen, A. Lagendijk, and A. Tip, Phys. Rev. Lett. **66**, 3132 (1991).

[23] A. Lagendijk, R. Vreeker, and P. de Vries, Phys. Lett. A **136**, 81 (1989); J.X. Zhu, D.J. Pine, and D.A. Weitz, Phys. Rev. A **44**, 3948 (1991).

[24] J.J. Duderstadt and L.J. Hamilton, *Nuclear Reactor Analysis* (Wiley, New York, 1976).

[25] M.S. Patterson, B. Chance, and B.C. Wilson, Appl. Opt. **28**, 2331 (1989).

[26] J. Shah, IEEE J. Quantum Electron. **24**, 276 (1988).